Potential COVID-19 papain-like protease PL^{pro} inhibitors: Repurposing FDA-approved drugs using a supercomputer

Valentina L Kouznetsova [1], **Aidan Zhang** [2], **Mahidhar Tatineni** [1], **Mark A Miller** [1], **Igor F Tsigelny** [Corresp. 1, 3, 4]

[1] San Diego Supercomputer Center, University of California, San Diego, La Jolla, California, United States

[2] REHS Program at San Diego Dupercomputer Center, University of California, San Diego, La Jolla, California, United States

[3] Department of Neurosciences, University of California, San Diego, La Jolla, California, United States

[4] Science, CureMatch Inc, San Diego, California, United States

Corresponding Author: Igor F Tsigelny
Email address: itsigeln@ucsd.edu

Using the crystal structure of SARS-CoV-2 papain-like protease (PL^{pro}) as a template, we developed a pharmacophore model of functional centers of the PL^{pro} inhibitor-binding pocket. With this model, we conducted data mining of the conformational database of FDA-approved drugs. This search identified 147 compounds that can be potential inhibitors of SARS-CoV-2 PL^{pro}. The conformations of these compounds underwent 3D fingerprint similarity clusterization, followed by docking of possible conformers to the binding pocket of PL^{pro}. Docking of random compounds to the binding pocket of protease was also done for comparison. Free energies of the docking interaction for the selected compounds were lower than for random compounds. The drug list obtained includes inhibitors of HIV, Hepatitis C, and cytomegalovirus (CMV), as well as a set of drugs that have demonstrated some activity in MERS, SARS-CoV, and SARS-CoV-2 therapy. We recommend testing of the selected compounds for treatment of COVID-19

Potential COVID-19 papain-like protease PL^{pro} inhibitors: Repurposing FDA-approved drugs

Valentina L. Kouznetsova[1], Aidan Zhang[2], Mahidhar Tatineni[1], Mark A. Miller[1], Igor F. Tsigelny[1,3,4*]

[1]San Diego Supercomputer Center, UC San Diego, Calif.

[2]REHS program, San Diego Supercomputer Center, UC San Diego, Calif.

[3]Curematch Inc., San Diego, Calif.

[4]Dept. of Neurosciences, UC San Diego, Calif.

*Correspondence to: itsigeln@ucsd.edu

Short Title: COVID-19 papain-like protease inhibitors: Repurposing FDA drugs.

ABSTRACT

Using the crystal structure of SARS-CoV-2 papain-like protease (PL^{pro}) as a template, we developed a pharmacophore model of functional centers of the PL^{pro} inhibitor-binding pocket. With this model, we conducted data mining of the conformational database of FDA-approved drugs. This search identified 147 compounds that can be potential inhibitors of SARS-CoV-2 PL^{pro}. The conformations of these compounds underwent 3D fingerprint similarity clusterization, followed by docking of possible conformers to the binding pocket of PL^{pro}. Docking of random compounds to the binding pocket of protease was also done for comparison. Free energies of the docking interaction for the selected compounds were lower than for random compounds. The drug list obtained includes inhibitors of HIV, Hepatitis C, and cytomegalovirus (CMV), as well as a set of drugs that have demonstrated some activity in MERS, SARS-CoV, and SARS-CoV-2 therapy. We recommend testing of the selected compounds for treatment of COVID-19.

One Sentence Summary: Using pharmacophore-based data mining and computational docking, we selected 147 potential COVID-19 papain-like protease inhibitors.

Introduction

Coronaviruses have caused the outbreak of several deadly respiratory diseases since the turn of the 21st century, such as the severe acute respiratory syndrome (SARS) in 2002 and the Middle East respiratory syndrome (MERS) in 2012, in addition to the recent COVID-19 pandemic, which has claimed more than 489 000 lives with over 9.5 million confirmed cases worldwide. Despite the profound impact of these viral outbreaks on public health and the economy, effective vaccines have not been found for either SARS or MERS viruses. In view of the ongoing pandemic, and the absence of vaccines, there is an immediate need to find drugs to treat patients.

Viral proteases are an attractive target for drug development. Viral proteases are essential for replication, and are unique to each virus, thus offering the potential for highly specific treatments that produce minimal toxic side effects. Viral protease inhibitors such as indinavir (HIV-1), ritonavir (HIV-1, HIV-2), and boceprevir (HCV) have been used to effectively treat a variety of viral infections [1]. For coronaviruses, extracellular proteases provide one possible target where protease inhibitors can prevent viral entry [2-4]. On the other hand, two viral proteases, PL^{pro} (papain-like protease) and $3CL^{pro}$ (chymotrypsin-like protease, aka main protease) are also attractive as druggable targets [5,6]. Both proteases are highly conserved domains of the specific nsps: nsp5 for $3CL^{pro}$ and nsp3 for PL^{pro}. Nsp3 is a large (200 000 kDa) multi-domain polypeptide that provides the membrane anchored scaffolding structure required for the replication/transcription complex (RTC) of coronaviruses [7]. In addition to PL^{pro}, the C-terminus of nsp3 contains transmembrane domains that anchor the protein and a dsDNA, unwinding/RNA binding domain that is essential for replicase activity [8]. It is a particularly attractive drug target because it plays an essential role in processing the viral polyproteins to create the mature nsp3, as well as helping the coronavirus evade host immune response via competitive interaction with ubiquitin and ISG15 on host-cell proteins [7,9-11]. Although no protease inhibitors are currently available for treatment of SARS, MERS, or COVID-19, studies of inhibitors of the MERS, SARS-CoV, and SARS-CoV-2 PL^{pro} are underway and reports have appeared that such protease inhibitors can prevent SARS-CoV replication in cultured cells [10,12-14].

In view of the urgent need for effective treatments and the high cost of developing new drugs (both in terms of time and resources), repurposing FDA-approved drugs is an efficient strategy for identifying drug candidates that can be used immediately in the COVID-19 pandemic [15]. In a previous report, we [16] and others [17-21] have used molecular modeling studies to identify FDA-approved drugs and other compounds [18,19,21,22] that are predicted to bind to $3CL^{pro}$. The list of potential inhibitors includes bleomycin, mithramycin, and goserelin, as well as others that may be effective [16]. Here we report a similar screen of FDA-approved drugs for potential inhibitors of SARS-COV-2 PL^{pro} using the recently reported structure of SARS-CoV-2 PL^{pro} (PDB ID: 6W9C) [23,24].

Methods

Pharmacophore design and use

Analyzing a pocket, we elucidated a majority of possible interactions between PL^{pro} (PDB ID: 6W9C) and a potential ligand for developing a protein-based pharmacophore model with potential fictional centers that would bind to the residues in the pocket (Figure 1A). Using Molecular Operating Environment (MOE; CCG, Montreal, Canada), we constructed two pharmacophore models including ten features (Pha01) and ten features with excluded volume R=1.3 Å (Pha02): two donors, two donors or acceptors, one hydrophobic, and five hydrophobic or aromatic features (Figure 1A). Based on developed pharmacophores to select potential drug-candidates, we conducted a pharmacophore search with both pharmacophore models on our conformational database (DB) of FDA-approved drugs, containing around 2500 drugs and 600 000 conformations. Searches were provided using pharmacophores partial match: eight of ten features for Pha01 and seven of ten features for Pha02. Search results of Pha01 (Search 1) identified 405 compounds with 63 821 conformations while Pha02 (Search 2) identified 857 compounds with 224 609 conformations. We selected 84 and 77 compounds from Search 1 and 2 respectively based on a number of H-bonds and hydrophobic interactions in the best docking pose. Because some compounds appeared in both searches, we eliminated duplicate compounds, resulting in a total of 147 unique drugs. Then we clustered the selected 147 compounds, using MOE Database Viewer with a fingerprint GpiDAPH3 and similarity–overlap parameter *SO* = 42% to elucidate the common structure-functional features of the groups of compound to enhance further drug development.

Docking of drug conformers using the supercomputer Comet

For docking the selected compounds, we used the crystal structure of the SARS-CoV-2 PLP (PDB ID: 6W9C). A binding pocket was defined based on the known residues of the S3/S4 binding pocket site of SARS-CoV-2 PLP. Docking of the selected compounds was done using Autodock Vina. Conformers of each of the selected compounds were generated using OpenBabel. However, since Autodock Vina does not support docking compounds that include boron atoms (i.e., bortezomib), each boron atom in the conformers of bortezomib was replaced with carbon atoms due to their similar size. The random control compounds were selected by a 79-compound, simple-random subset of all the ZINC DB compounds; these were docked with PL^{pro} in the same processes. Likewise, the conformers of the compound with ID: ZINC001779539170 had their silicon atom replaced with carbon due to Autodock Vina's restraints regarding supported atoms.

The Comet supercomputer at the San Diego Supercomputer Center (SDSC) was primarily used for two parts of the analyses: (1) conversion of files in the pdb format to the pdbqt format, using the Open Babel software (version 2.4.1), and (2) all the docking computations using the AutoDock Vina software (version 1.1.2). We outline the system configuration and the analyses workflow details below.

The Comet supercomputing system

Comet is an NSF funded cluster (NSF grant: ACI #1341698) designed by Dell and SDSC delivering 2.76 peak petaflops. It features Intel Haswell processors with AVX2, Mellanox FDR InfiniBand interconnects, and Aeon storage [25]. There are 1944 standard compute nodes and 72 GPU nodes. The standard compute nodes consist of Intel Xeon E5-2680v3 (Haswell) processors, 128 GB DDR4 DRAM (64 GB per socket), and 320 GB of SSD local scratch memory. The GPU nodes contain four NVIDIA GPUs each. There are four large memory nodes containing 1.5 TB of DRAM and four Haswell processors each. All the computations for this paper were conducted on the standard compute nodes and made extensive use of the local scratch filesystems.

File conversion and docking workflow

The first step in the computational workflow on Comet was to convert 385 193 pdb files of drug conformers into the pdbqt format. The files were contained in 27 zip files and the jobs were simultaneously run on Comet (one zip file in each job). The zip files were extracted to the local

SSD based file system to reduce IO loads, converted to pdbqt files in the same location, and then the results were archived in a zip file. With the local SSD approach, all the conversion jobs were completed in less than 20 minutes.

The AutoDock Vina software was used to dock a total of 490 678 drug conformers using computations on Comet. The local SSD approach was used again to mitigate IO loads on the main filesystem. The docking tasks were split up into separate jobs (that were run simultaneously) with 3000–4000 drug conformers docked in each job. All the individual docking computations were conducted using 8 cores (The parallelism is limited by the exhaustiveness parameter, set to 8 for the analysis) and scaling tests showed an excellent parallel efficiency of 93.2%.

Results

Among the compounds selected by the pharmacophore search of FDA-approved drug DB, we identified two clusters (A and B) containing twenty compounds; three clusters (C, D, and E) containing nine, five, and ten compounds correspondingly; two clusters (F and G) with four, and three clusters (H, I, and J) with three compounds; along with ten two-compounds clusters and 46 not clustered single compounds. Compounds in clusters A–G are listed in Table 1, other compounds can be found in Supplemental Materials (Table S1). Flexible alignment of clusters B and C were used to illustrate compounds' common features (Figure 2).

Figure 1. Insert here

Interesting to note that this selection contained the best docking energy drug nilotinib that showed activity against SARS-CoV.

Table 1. Insert here

Figure 2A and B shows the flexible alignments of clusters B and C containing the drugs with the best docking energies.

Figure 2. Insert here

To define the putative best binding drugs, we conducted docking of multiple conformers of drugs selected from a pharmacophore-based search and of random compounds to the binding site of COVID-19 papain-like protease. The random control compounds were selected by a 79-compound, simple-random subset of the ZINC DB of drug-like compounds. For docking the selected compounds, we used the same crystal structure of the SARS-CoV-2 (Protein Data Bank entry, 6W9C) imported into MOE. A S3/S4 pocket site was defined, which included the following residues: K157, L162, G163, D164, R166, P247, P248, Y264, G266, Y268, and P299. Conformers of each of the selected compounds were generated with OpenBabel before being docked with AutoDock Vina.

Figure 3 shows the values of docking free energies of the selected and random compounds. The energies of interaction with PL^{pro} are shown in Table 2. One can see that drugs of clusters 2 and 5 are at the top of the table. Note that the binding pocket of PL^{pro} is not very specific and contains a number of hydrophobic binding centers; that is why binding energies are not overwhelmingly better than those of random compounds (Figure 3). At the same time, we want also note that the values of energies in the table can be used with discretion. Binding positions of ligands in the pockets of proteins in many cases do not have minimal energies.

Figure 3. Inset here

Table 2. Insert here

Figure 4. Insert here

Discussion

Based on the crystal structure of SARS-CoV-2 PL^{pro} (PDB ID: 6W9C), we developed two pharmacophore models of the binding pocket of this protein. Using these models, we browsed our conformational database of FDA-approved drugs and obtained 147 hits that were clusterized for selecting the most promising candidates and then used for multi-conformational docking to the PL^{pro} pocket. The drug list obtained includes inhibitors of HIV, Hepatitis C, and CMV, as well as a set of drugs that demonstrated some activity in MERS, SARS-CoV, and SARS-CoV-2 therapy. We developed a pharmacophore model of the binding pocket site S3/S4 of COVID-19 PL^{pro} then

conducted multi-conformational docking of these drug compounds to this site for ranging the potential inhibitors selected by pharmacophore-based search. We also conducted clusterization of the selected compounds based on their pharmacophores 3D profiles to elucidate the common features for further drug design, and compared the docking results for the selected drug compounds with the docking results of random compounds to evaluate the area of significance in the values of binding energies. We note that the pharmacophore-based selection is a very powerful tool so even the drugs with the binding energies on the same level with the random compound do not have to be completely discarded.

We are aware of two other studies where docking experiments were used to predict binding of existing pharmaceuticals to the SARS-CoV-2 PL^{pro} [9,18]. Both prior studies relied on homology modelling of part [18] or the entire SARS-CoV PL^{pro}. Wu et al [18] studied 2924 compounds from ZINC Drug Database, as well as 78 known antivirals; while Arya et al. studied 2525 FDA-approved compounds from DrugBank and the ZINC 15 database. Two compounds were identified in the present study and by Wu et al [9]: valganciclovir and pemextred. The remaining compounds identified here are unique to our study. This may reflect the influence of using the crystal structure of SARS-CoV-2 as the starting point in the present study, and a difference in methodology in our case including preliminary pharmacophore-based search before docking computational experiments.

It is interesting to note that several drugs with high docking energy were tested or are in experimental testing: nilotinib was active only for SARS-CoV [26]; dasatinib was confirmed to be active in cell-culture assays for MERS-CoV and SARS-CoV [27]. Dasatinib was also shown to be active against SARS-Cov-2 in clinical cases [27]. Terconazole and fluspirilene were shown to be active in cell-culture assays for SARS-Cov-2 [27]. Manidipine was found in the database of experimental results for broad set of antiviral drugs, DrugVirus.info [28]. Indinavir and ritonavir (HIV viral protease inhibitor), boceprevir (Hepatitis C protease inhibitor), and valganciclovir (antiviral medication for CMV) were found with energies of binding to PL^{pro} of −6.7 kcal/mol and better. We note that according to the DrugVirus.info database [28], 11 of the compounds selected by the pharmacophore-based search showed activity against the set of viruses (Fig. 4) including amodiaquine, chloroquine, sorafenib, dasatenib, hydroxychloroquine, bortezomib, topotecan, manidipine, lovastatin, gefitinib, and ritonavir. Most experimental testing was done in cell-cultures, but there is also a significant amount of animal testing and several of these drugs are in

different stages of clinical trials. The prior computational studies [9,18] did not identify any of these compounds as potential inhibitors of PL^{pro}, with the exception of chloroquine [18]. On the other hand, Wu et al. [9] identified two antivirals that our experiments did not predict as inhibitors: ribavirin and β-thymidine.

Acknowledgements

We would like to thank the people of San Diego Supercomputer Center and CureMatch, Inc., for friendly support.

Funding: The SDSC Comet supercomputer is supported by the NSF grant: ACI #1341698 Gateways to Discovery: Cyberinfrastructure for the Long Tail of Science. MAM was supported by NIH R01 GM126463.

Author contributions: IFT and VLK introduced initial idea of the project; VLK conducted pharmacophore development, databases searches, and clustering and multiconfromational alignment; MAM, IFT, and VLK conducted interpretation of the results AZ and MT conducted computational docking on Comet supercomputer; IFT, VLK, MAM, and AZ wrote the article.

Competing interests: Authors declare no competing interests.

References

1. Anderson, J., Schiffer, C., Lee, S.-K., and Swanstrom, R. (2009) Viral Protease Inhibitors. in *Antiviral Strategies* (Kräusslich, H.-G., and Bartenschlager, R. eds.), Springer Berlin Heidelberg, Berlin, Heidelberg. pp 85–110. 10.1007/978-3-540-79086-0_4

2. Hoffmann, M., Kleine-Weber, H., Schroeder, S., Krüger, N., Herrler, T., Erichsen, S., Schiergens, T. S., Herrler, G., Wu, N. H., Nitsche, A., Müller, M. A., Drosten, C., and Pöhlmann, S. (2020) SARS-CoV-2 Cell Entry Depends on ACE2 and TMPRSS2 and Is Blocked by a Clinically Proven Protease Inhibitor. *Cell* **181**, 271–280.e278. 10.1016/j.cell.2020.02.052

3. Simmons, G., Gosalia, D. N., Rennekamp, A. J., Reeves, J. D., Diamond, S. L., and Bates, P. (2005) Inhibitors of cathepsin L prevent severe acute respiratory syndrome coronavirus entry. *Proc Natl Acad Sci U S A* **102**, 11876–11881. 10.1073/pnas.0505577102

4. Zhou, Y., Vedantham, P., Lu, K., Agudelo, J., Carrion, R., Jr., Nunneley, J. W., Barnard, D., Pöhlmann, S., McKerrow, J. H., Renslo, A. R., and Simmons, G. (2015) Protease inhibitors targeting coronavirus and filovirus entry. *Antiviral research* **116**, 76–84. 10.1016/j.antiviral.2015.01.011

5. Vuong, W., Khan, M. B., Fischer, C., Arutyunova, E., Lamer, T., Shields, J., Saffran, H. A., McKay, R. T., van Belkum, M. J., Joyce, M., Young, H. S., Tyrrell, D. L., Vederas, J. C., and Lemieux, M. J. (2020) Feline coronavirus drug inhibits the main protease of SARS-CoV-2 and blocks virus replication. *bioRxiv*, 2020.2005.2003.073080. 10.1101/2020.05.03.073080

6. Ma, C., Sacco, M. D., Hurst, B., Townsend, J. A., Hu, Y., Szeto, T., Zhang, X., Tarbet, B., Marty, M. T., Chen, Y., and Wang, J. (2020) Boceprevir, GC-376, and calpain inhibitors II, XII inhibit

SARS-CoV-2 viral replication by targeting the viral main protease. *bioRxiv*, 2020.2004.2020.051581. 10.1101/2020.04.20.051581

7. Lei, J., Kusov, Y., and Hilgenfeld, R. (2018) Nsp3 of coronaviruses: Structures and functions of a large multi-domain protein. *Antiviral Research* **149**, 58–74. https://doi.org/10.1016/j.antiviral.2017.11.001

8. Neuman, B. W. (2016) Bioinformatics and functional analyses of coronavirus nonstructural proteins involved in the formation of replicative organelles. *Antiviral Research* **135**, 97–107. https://doi.org/10.1016/j.antiviral.2016.10.005

9. Wu, C., Liu, Y., Yang, Y., Zhang, P., Zhong, W., Wang, Y., Wang, Q., Xu, Y., Li, M., Li, X., Zheng, M., Chen, L., and Li, H. (2020) Analysis of therapeutic targets for SARS-CoV-2 and discovery of potential drugs by computational methods. *Acta Pharmaceutica Sinica B* **10**, 766–788. https://doi.org/10.1016/j.apsb.2020.02.008

10. Báez-Santos, Y. M., St. John, S. E., and Mesecar, A. D. (2015) The SARS-coronavirus papain-like protease: Structure, function and inhibition by designed antiviral compounds. *Antiviral Research* **115**, 21–38. https://doi.org/10.1016/j.antiviral.2014.12.015

11. Lei, J., Mesters, J. R., Drosten, C., Anemüller, S., Ma, Q., and Hilgenfeld, R. (2014) Crystal structure of the papain-like protease of MERS coronavirus reveals unusual, potentially druggable active-site features. *Antiviral Research* **109**, 72–82. https://doi.org/10.1016/j.antiviral.2014.06.011

12. Ratia, K., Pegan, S., Takayama, J., Sleeman, K., Coughlin, M., Baliji, S., Chaudhuri, R., Fu, W., Prabhakar, B. S., Johnson, M. E., Baker, S. C., Ghosh, A. K., and Mesecar, A. D. (2008) A noncovalent class of papain-like protease/deubiquitinase inhibitors blocks SARS virus replication. *Proceedings of the National Academy of Sciences* **105**, 16119–16124. 10.1073/pnas.0805240105

13. Lee, H., Lei, H., Santarsiero, B. D., Gatuz, J. L., Cao, S., Rice, A. J., Patel, K., Szypulinski, M. Z., Ojeda, I., Ghosh, A. K., and Johnson, M. E. (2015) Inhibitor recognition specificity of MERS-CoV papain-like protease may differ from that of SARS-CoV. *ACS Chem Biol* **10**, 1456–1465. 10.1021/cb500917m

14. Akaji, K., Konno, H., Mitsui, H., Teruya, K., Shimamoto, Y., Hattori, Y., Ozaki, T., Kusunoki, M., and Sanjoh, A. (2011) Structure-Based Design, Synthesis, and Evaluation of Peptide-Mimetic SARS 3CL Protease Inhibitors. *Journal of Medicinal Chemistry* **54**, 7962–7973. 10.1021/jm200870n

15. Tan, E., L. C. , Ooi, E. E., Lin, C.-Y., Tan, H. C., Ling, A. E., Lim, B., and Stanton, L., W. (2004) Inhibition of SARS Coronavirus Infection In Vitro with Clinically Approved Antiviral Drugs. *Emerging Infectious Disease journal* **10**, 581. 10.3201/eid1004.030458

16. Kouznetsova, V., Huang, D., and Tsigelny, I. F. (2020) Potential COVID-19 Protease Inhibitors: Repurposing FDA approved Drugs. *ChemRxiv* 10.26434/chemrxiv.12093900.v1

17. Kandeel, M., and Al-Nazawi, M. (2020) Virtual screening and repurposing of FDA approved drugs against COVID-19 main protease. *Life Sciences* **251**, 117627. https://doi.org/10.1016/j.lfs.2020.117627

18. Arya, R., Das, A., Prashar, V., and Kumar, M. (2020) *Potential Inhibitors Against Papain-like Protease of Novel Coronavirus (COVID-19) from FDA Approved Drugs*, 10.26434/chemrxiv.11860011

19. Liu, X., and Wang, X.-J. (2020) Potential inhibitors for 2019-nCoV coronavirus M protease from clinically approved medicines. *bioRxiv*, 2020.2001.2029.924100. 10.1101/2020.01.29.924100

20. Plewczynski, D., Hoffmann, M., Von Grotthuss, M., Ginalski, K., and Rychewski, L. (2007) In Silico Prediction of SARS Protease Inhibitors by Virtual High Throughput Screening. *Chemical Biology & Drug Design* **69**, 269–279. 10.1111/j.1747-0285.2007.00475.x

21. Ton, A.-T., Gentile, F., Hsing, M., Ban, F., and Cherkasov, A. (2020) Rapid Identification of Potential Inhibitors of SARS-CoV-2 Main Protease by Deep Docking of 1.3 Billion Compounds. *Molecular Informatics* **n/a**10.1002/minf.202000028

22. Alamri, M. A., Tahir ul Qamar, M., and Alqahtani, S. M. (2020) Pharmacoinformatics and Molecular Dynamic Simulation Studies Reveal Potential Inhibitors of SARS-CoV-2 Main Protease 3CLpro. *Preprints 2020, 2020020308* 10.20944/preprints202002.0308.v1

23. Zhang, L., Lin, D., Sun, X., Curth, U., Drosten, C., Sauerhering, L., Becker, S., Rox, K., and Hilgenfeld, R. (2020) Crystal structure of SARS-CoV-2 main protease provides a basis for design of improved α-ketoamide inhibitors. *Science* **368**, 409–412. 10.1126/science.abb3405

24. Osipiuk, J., Jedrzejczak, R., Tesar, C., Endres, M., Stols, L., Babnigg, G., Kim, Y., Michalska, K., and Joachimiak, A. (2020) The crystal structure of papain-like protease of SARS CoV-2, 2020. 10.2210/pdb6W9C/pdb

25. Richard L. Moore, Chaitan Baru, Diane Baxter, Geoffrey C. Fox, Amit Majumdar, Phillip Papadopoulos, Wayne Pfeiffer, Robert S. Sinkovits, Shawn Strande, Mahidhar Tatineni, Richard P. Wagner, Nancy Wilkins-Diehr, and Michael L. Norman. 2014. Gateways to Discovery: Cyberinfrastructure for the Long Tail of Science. In Proceedings of the 2014 Annual Conference on Extreme Science and Engineering Discovery Environment (XSEDE '14). Association for Computing Machinery, New York, NY, USA, Article 39, 1–8. DOI:https://doi.org/10.1145/2616498.2616540

26 Dyall J, Coleman CM, Hart BJ, et al. (2014). Repurposing of clinically developed drugs for treatment of Middle East respiratory syndrome coronavirus infection. *Antimicrobial Agents and Chemotherapy* 58, 8, 4885–4893

27 Abruzzese E., Luciano L., D'Agostino F., Trawinska M. M., Pane F., De Fabritiis P. SARS-CoV-2 (COVID-19) and Chronic Myeloid Leukemia (CML): a case report and review of ABL kinase involvement in infection. *Mediterr J Hematol Infect Dis* 2020, 12(1): e2020031, DOI: http://dx.doi.org/10.4084/MJHID.2020.031

28 Andersen PI, Ianevski A, Lysvand H, Vitkauskiene A, et al. Discovery and Development of Safe-In-Man Broad-Spectrum Antiviral Agents. *Int J Infect Dis*. 2020 Apr;93:268–276. doi: 10.1016/j.ijid.2020.02.018.

Figure Legends.

Figure 1. Binding position of the drugs with the best scores in papain-like protease. **(A)** Ten features pharmacophore. The model contains ten functional centers: two donors, two donors or acceptor centers, one hydrophobic center, and five hydrophobic or aromatic centers (excluded volume is hidden). **(B)** Dihydroergocryptine, docking free energy (DFE) = −8.0 kcal/mol. **(C)** Enasidenib, (DFE) = −8.1 kcal/mol. **(D)** Irinotecan, (DFE) = −8.5 kcal/mol. **(E)** Levomefolic acid, (DFE) = −8.4 kcal/mol. **(F)** Nilotinib, (DFE) = −9.3 kcal/mol. **(G)** Siponimod, (DFE) = −8.0 kcal/mol. **(H)** Sorafenib, (DFE) = −8.0 kcal/mol.

Figure 2. Flexible alignments of compounds in clusters selected by the pharmacophore-based search of possible drug-candidates in the conformational database of FDA-approved drugs having the best docking energies. **(A)** Cluster B (20 compounds), **(B)** cluster C (9 compounds).

Figure 3. Free energies of docking interactions of selected and random compounds with PL^{pro}. Minimal energies of the selected and random compounds are −9.3 and −7.7 kcal/mol respectively.

Figure 4. Drugs among the predicted by pharmacophore search inhibitors of PL^{pro} that were experimentally tested for various viruses (Obtained using DrugVirus.info database [26]).

Figure 1

Ten features pharmacophore of papin-like protease binding pocket..

The model contains ten functional centers: two donors, two donors or acceptor centers, one hydrophobic center, and five hydrophobic or aromatic centers (excluded volume is hidden).

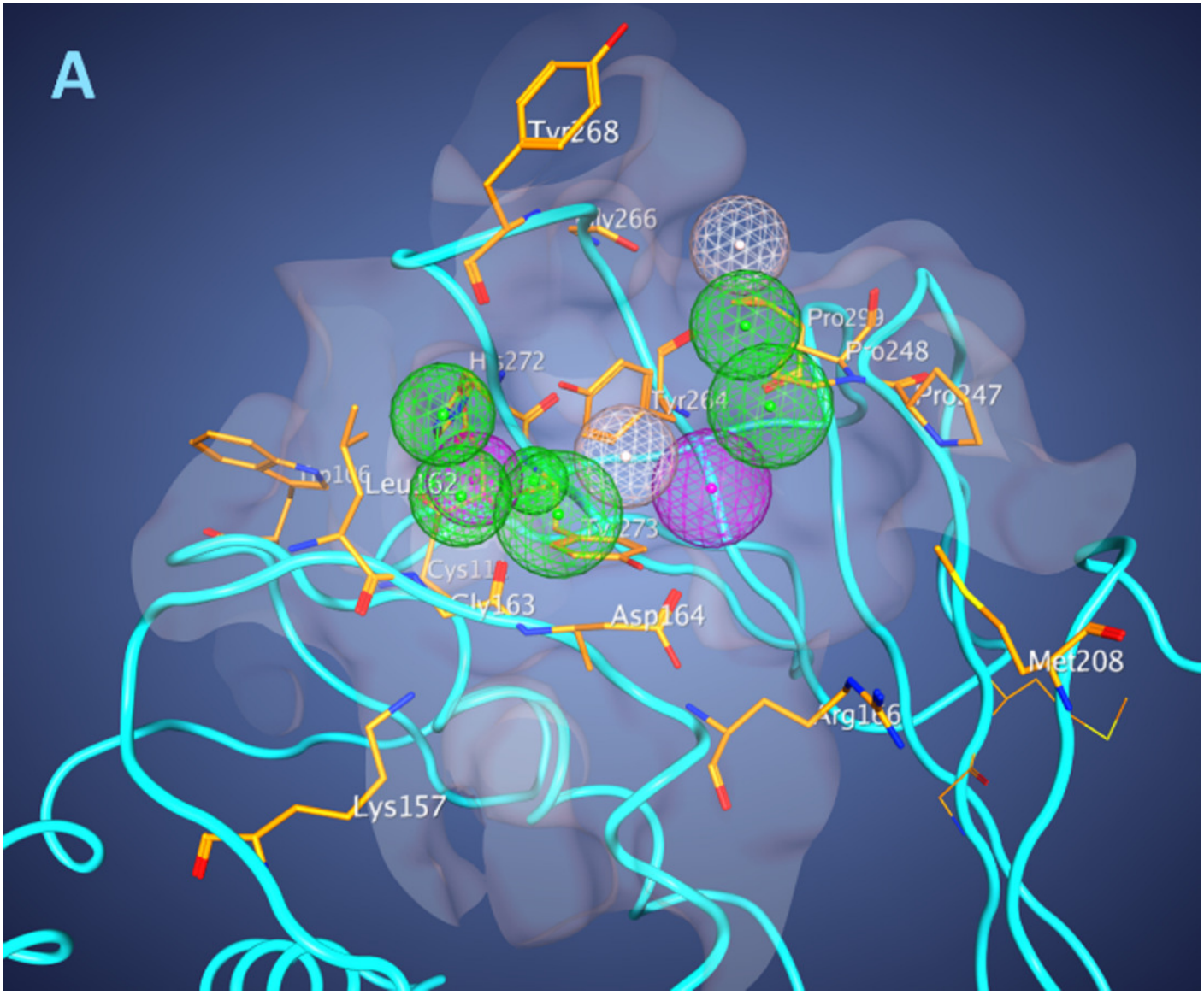

Figure 2

Binding position of the drugs with the best scores in papain-like protease.

Dihydroergocryptine, docking free energy (DFE) = −8.0 kcal/mol.

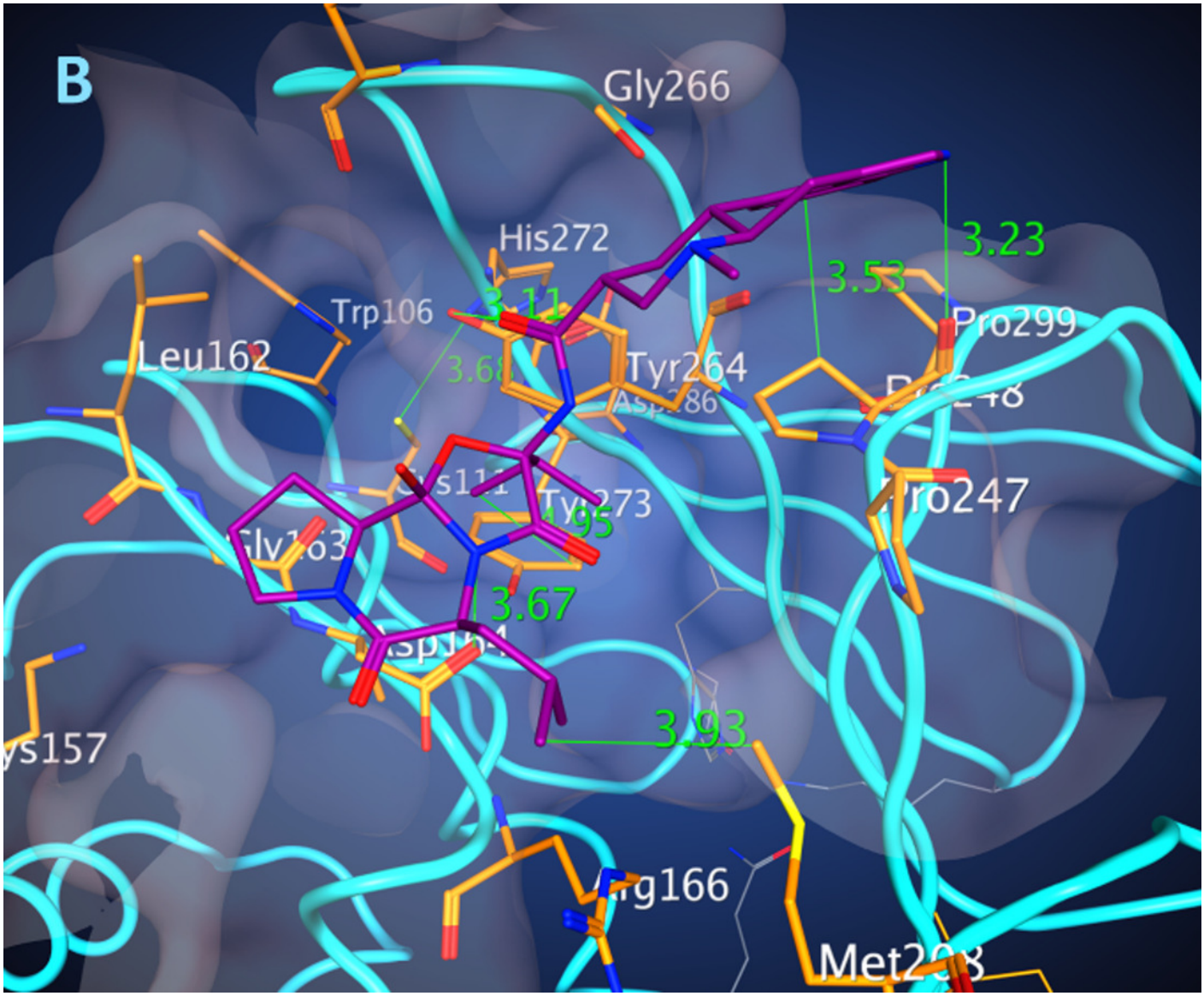

Figure 3

Binding position of the drugs with the best scores in papain-like protease.

Enasidenib, (DFE) = −8.1 kcal/mol.

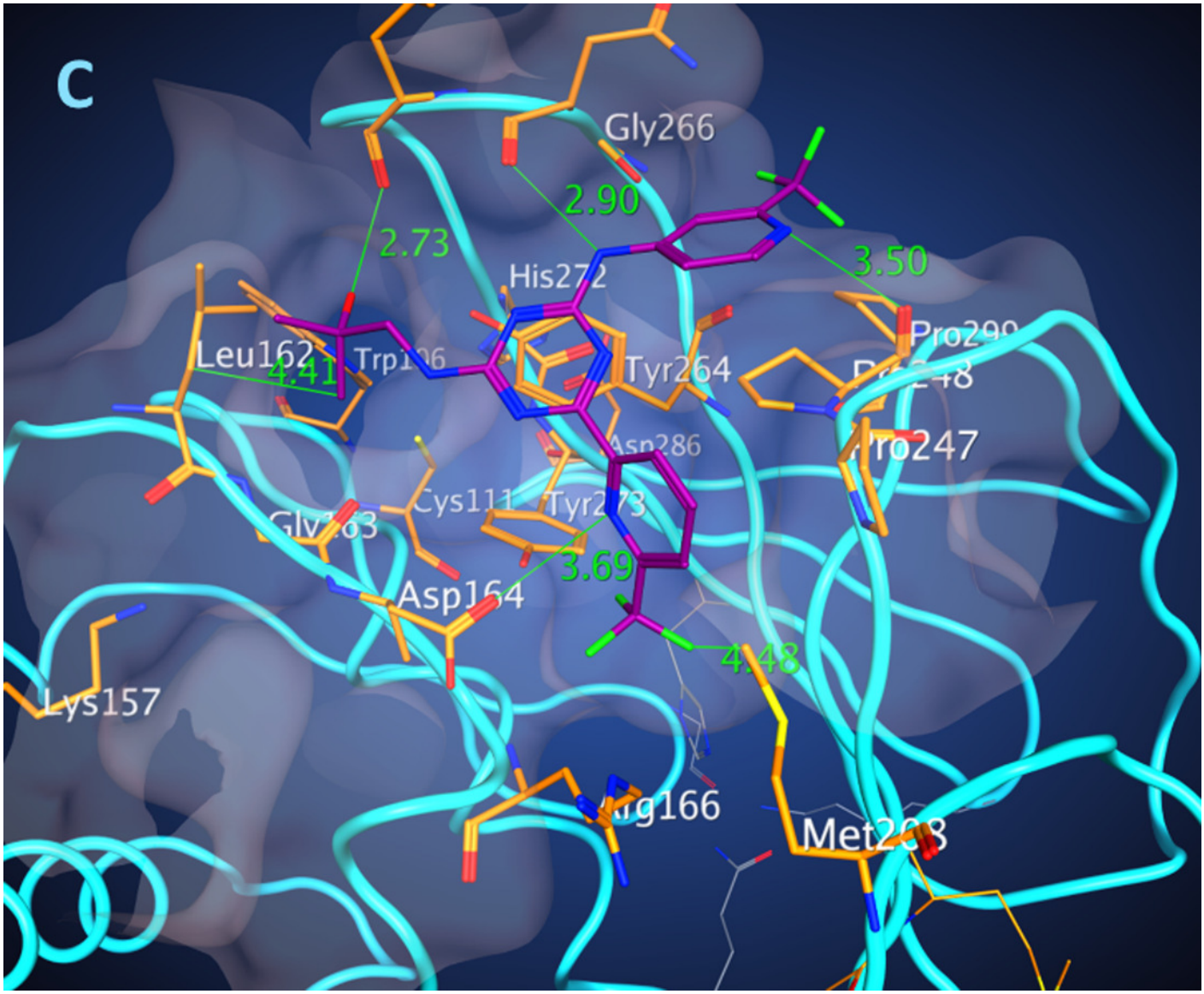

Figure 4

Binding position of the drugs with the best scores in papain-like protease.

Irinotecan, (DFE) = −8.5 kcal/mol.

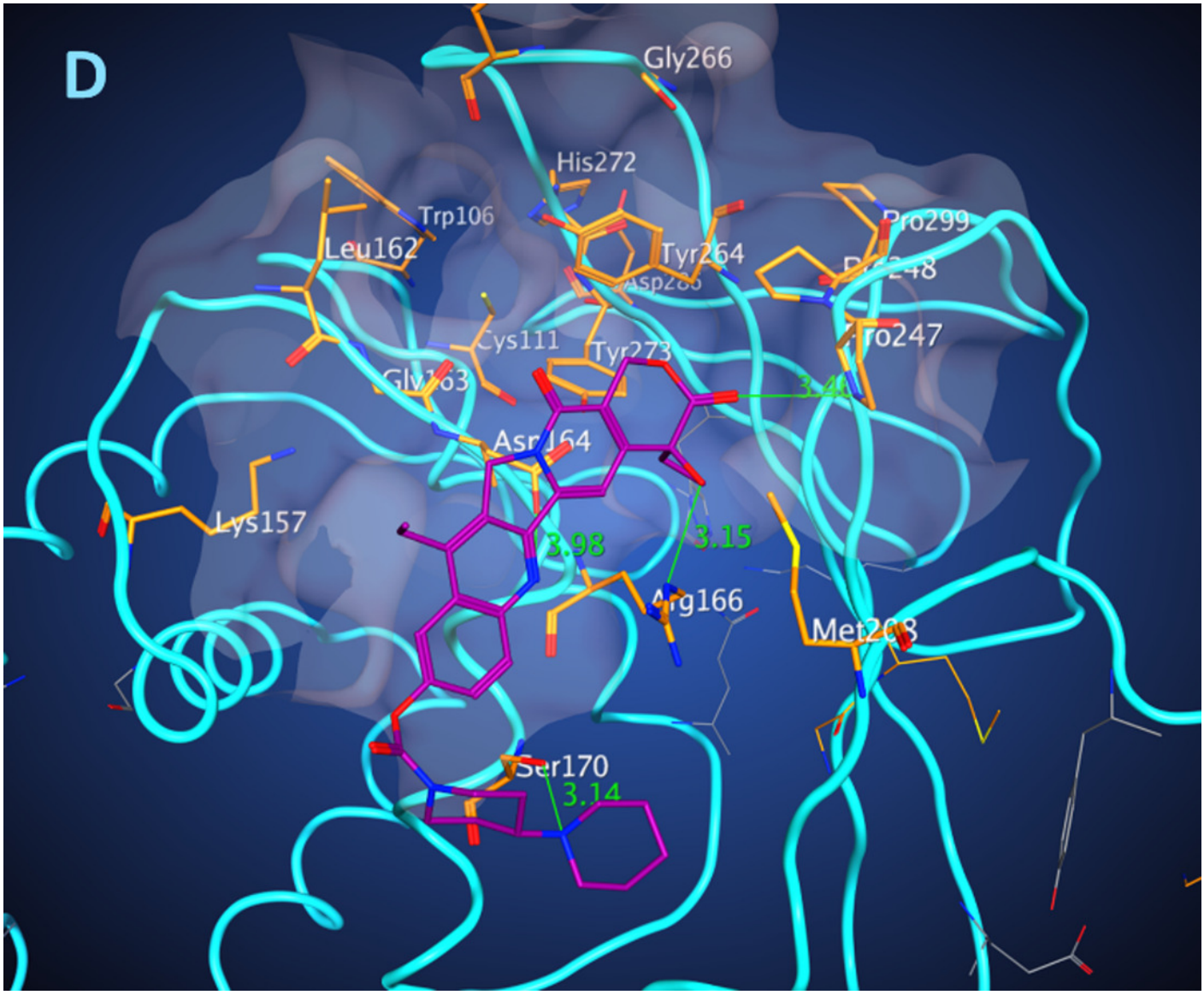

Figure 5

Binding position of the drugs with the best scores in papain-like protease. (A) Ten features pharmacophore.

Levomefolic acid, (DFE) = −8.4 kcal/mol.

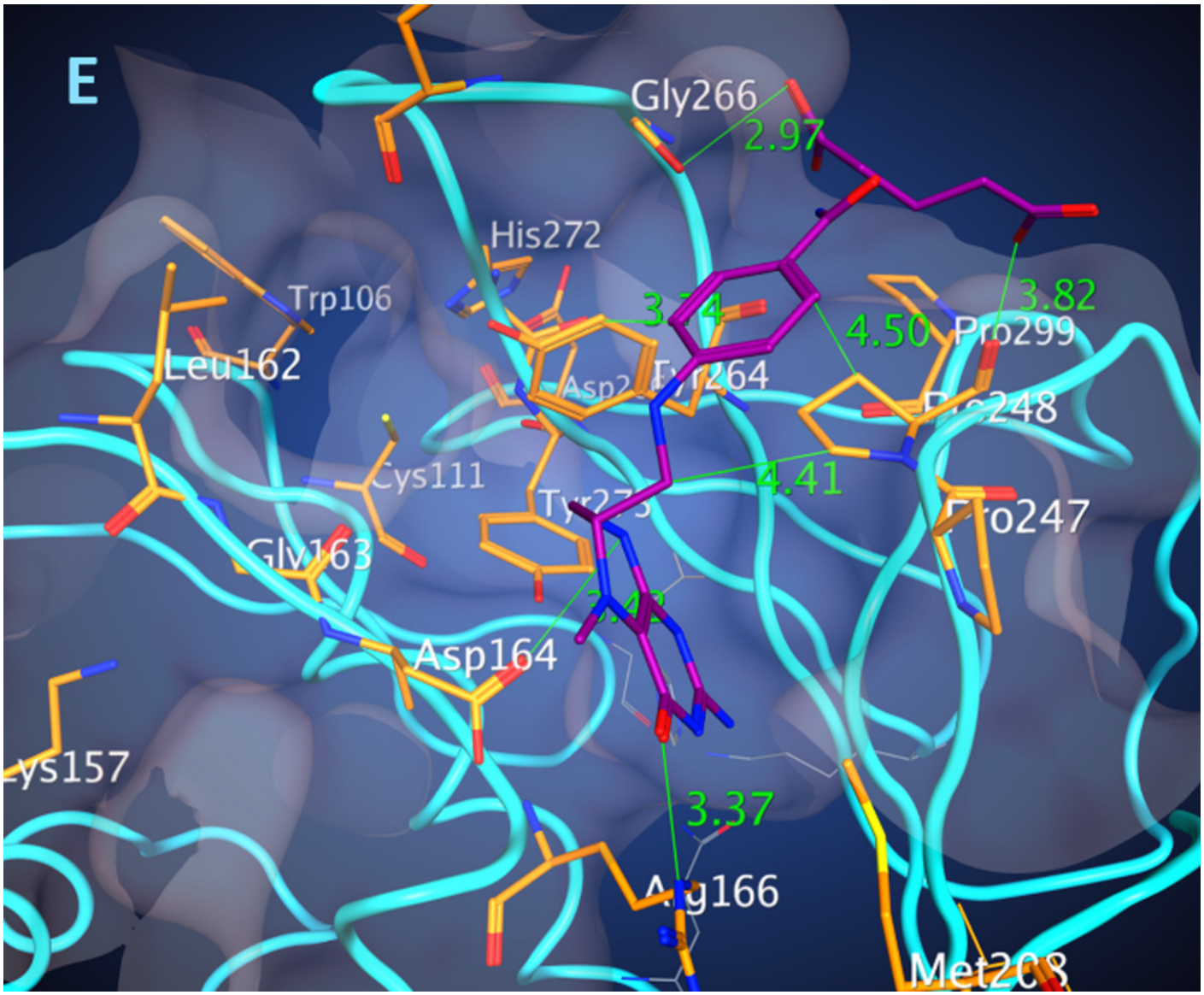

Figure 6

Binding position of the drugs with the best scores in papain-like protease. (A) Ten features pharmacophore.

Nilotinib, (DFE) = −9.3 kcal/mol.

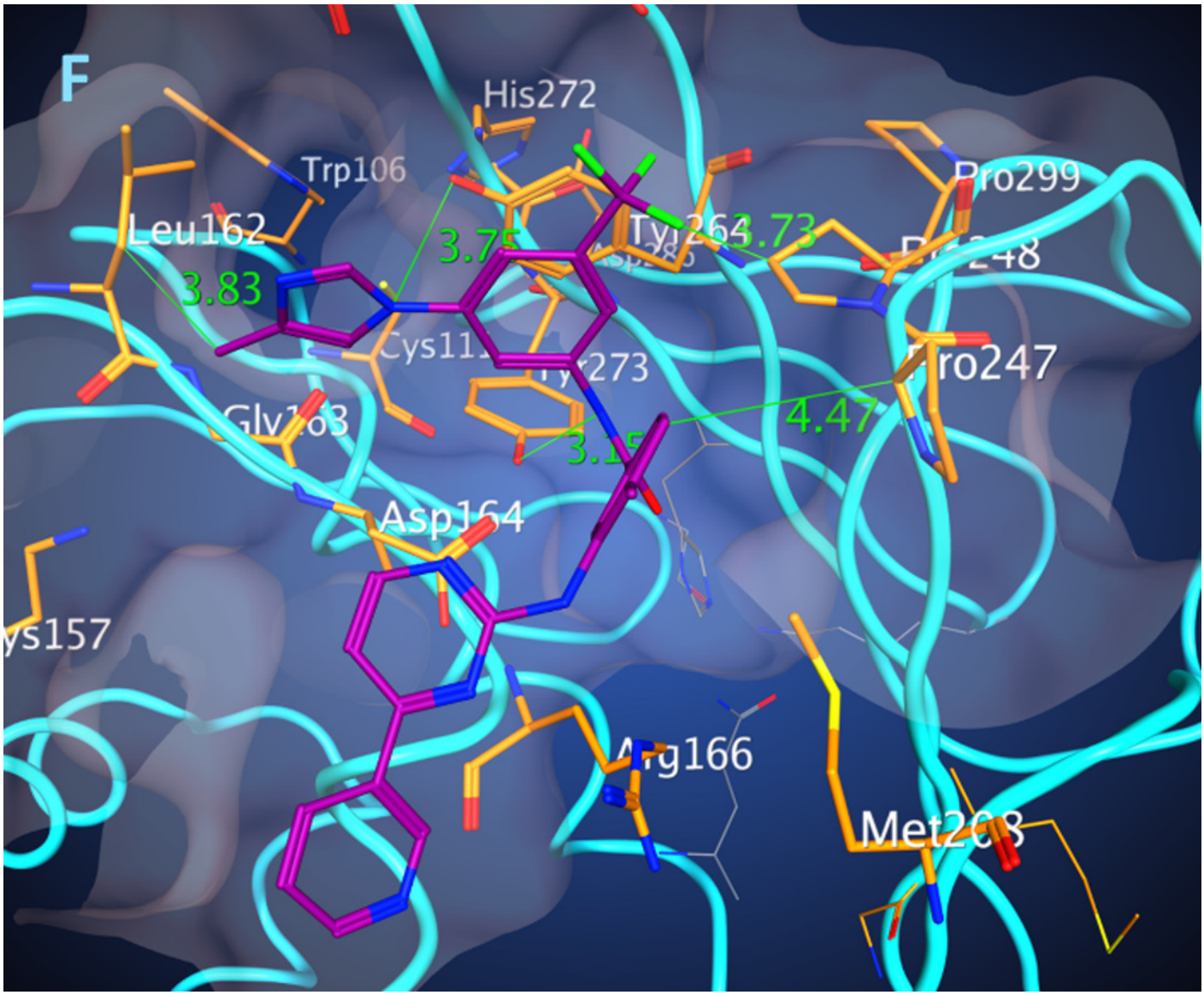

Figure 7

Binding position of the drugs with the best scores in papain-like protease. (A) Ten features pharmacophore.

Siponimod, (DFE) = −8.0 kcal/mol.

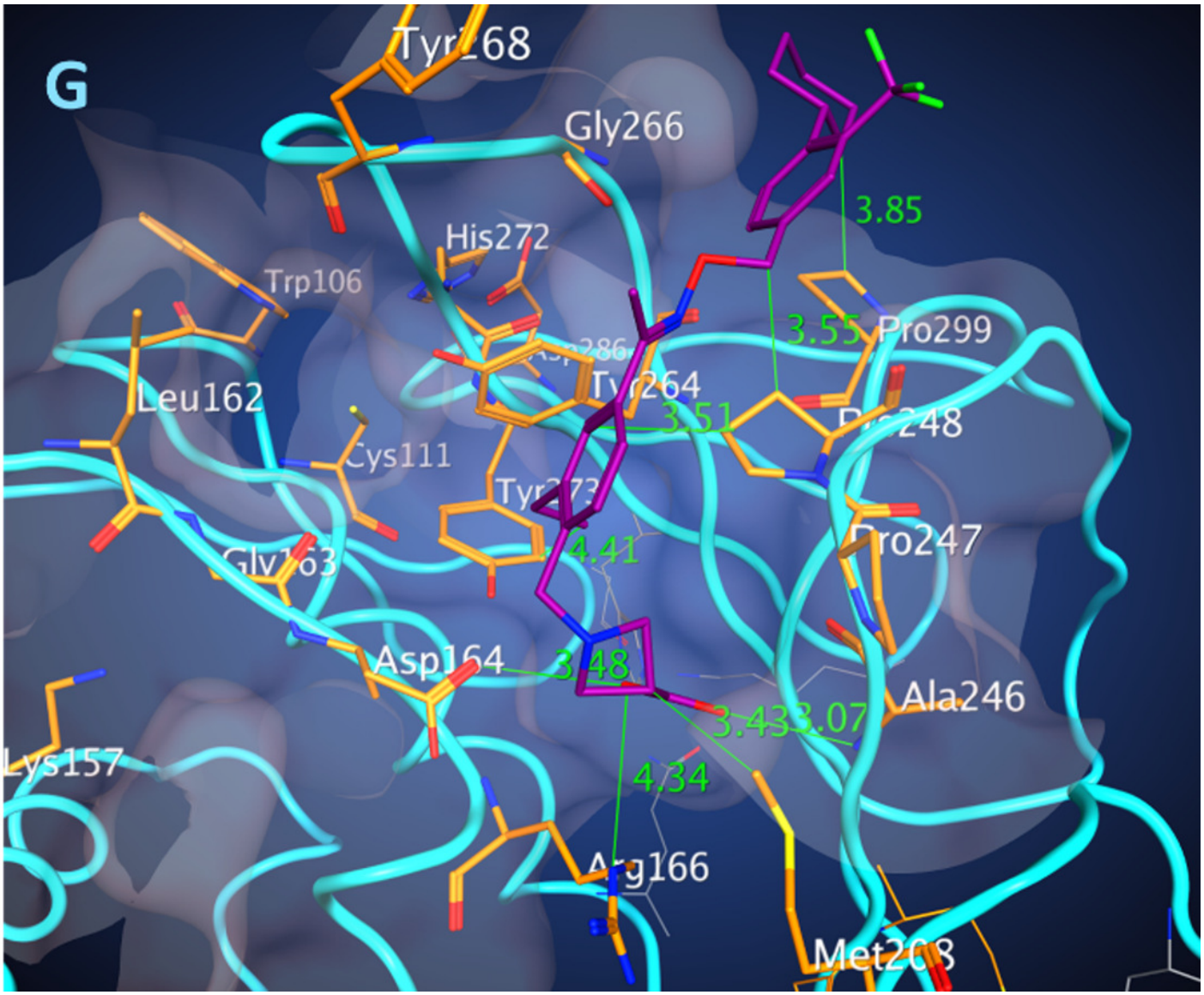

Figure 8

Binding position of the drugs with the best scores in papain-like protease.

Sorafenib, (DFE) = −8.0 kcal/mol.

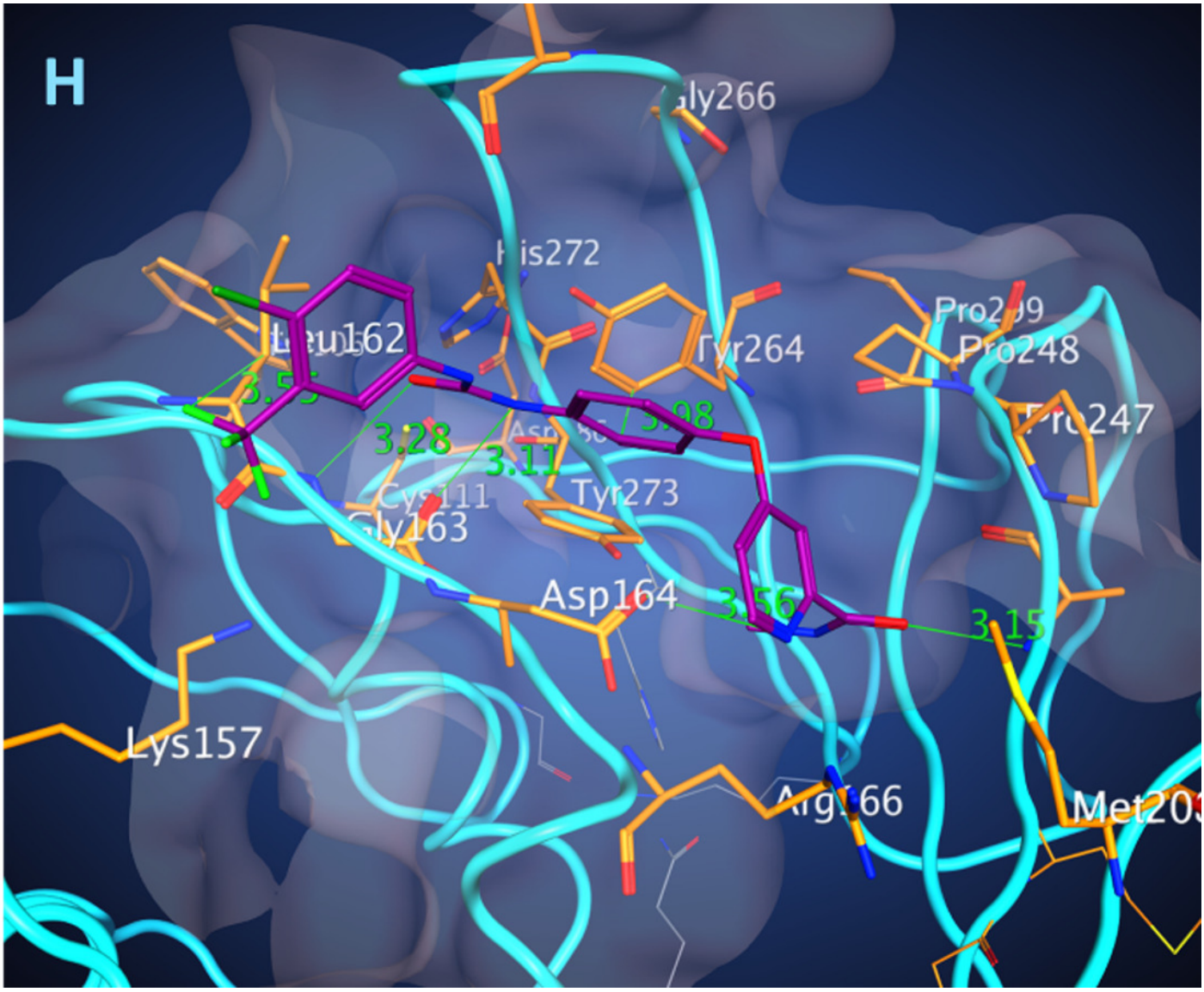

Figure 9

Flexible alignments of compounds in clusters selected by the pharmacophore-based search of possible drug-candidates in the conformational database of FDA-approved drugs having the best docking energies.

Cluster B (20 compounds)

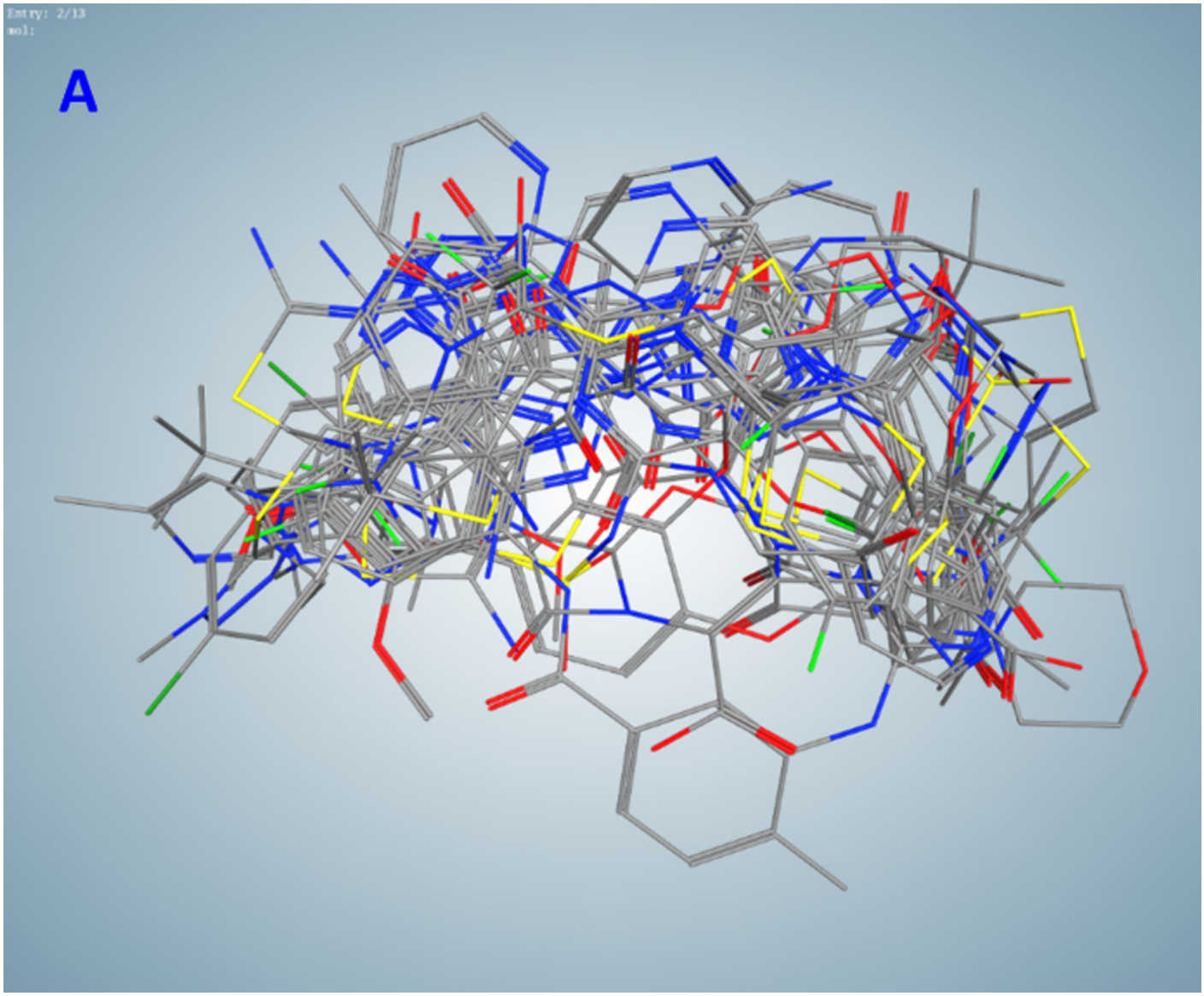

Figure 10

Flexible alignments of compounds in clusters selected by the pharmacophore-based search of possible drug-candidates in the conformational database of FDA-approved drugs having the best docking energies.

Cluster C (9 compounds).

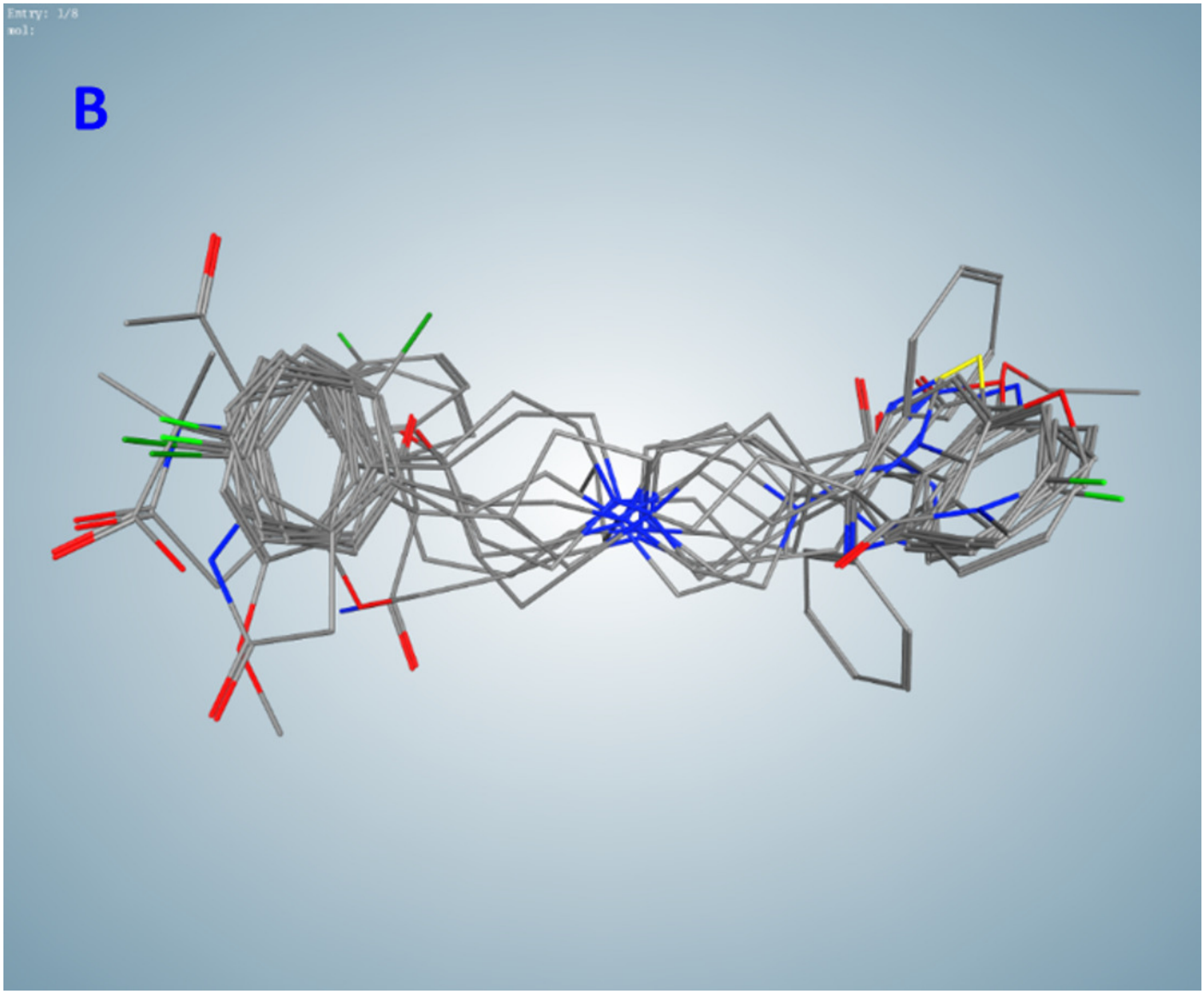

Figure 11

Free energies of docking interactions of selected and random compounds with PL^{pro}.

Minimal energies of the selected and random compounds are −9.3 and −7.7 kcal/mol respectively.

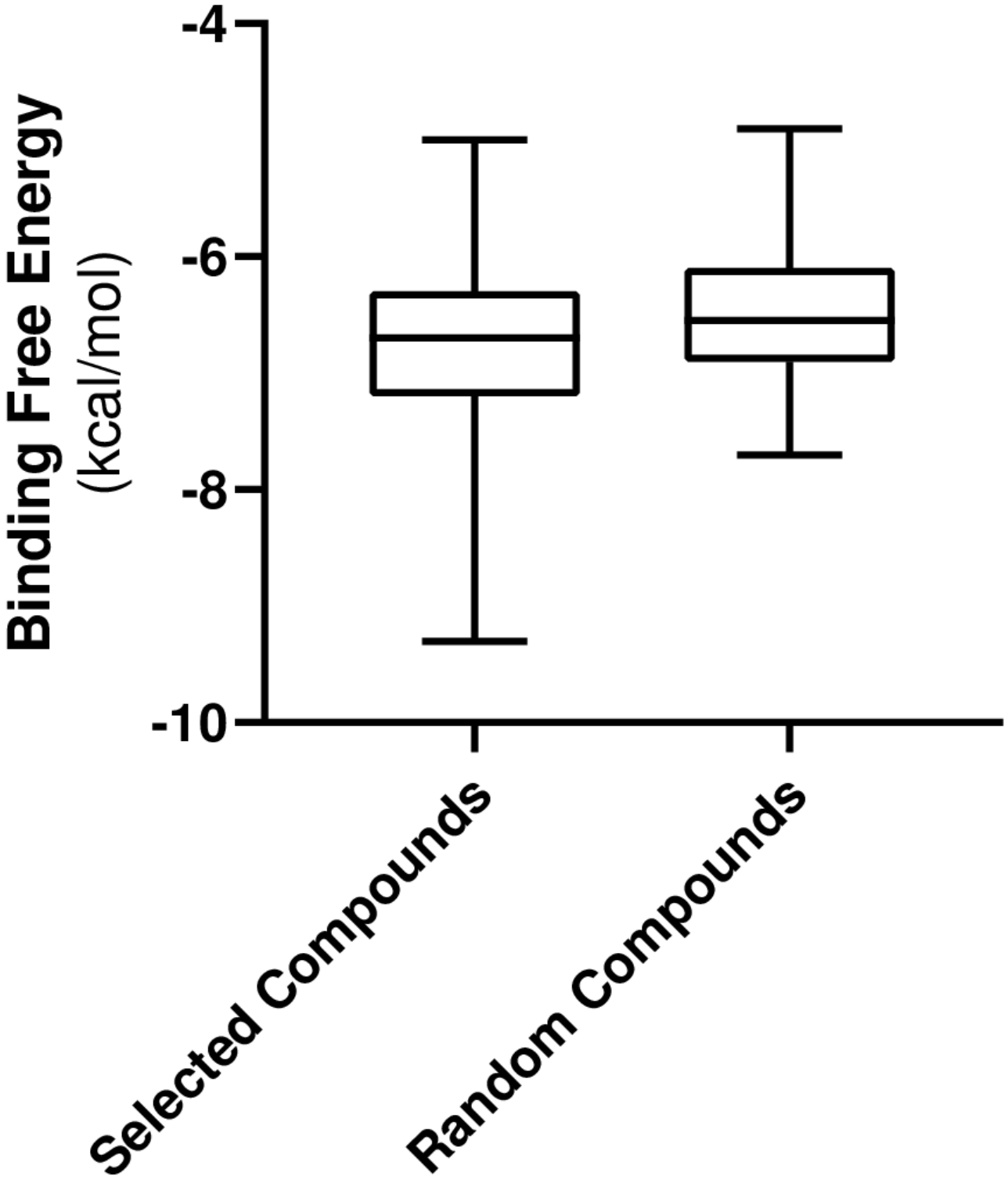
Binding Free Energy
(kcal/mol)
-4
-6
-8
-10
Selected Compounds
Random Compounds

Figure 12

Drugs among the predicted by pharmacophore search inhibitors of PL^{pro} that were experimentally tested for various viruses

Obtained using DrugVirus.info database [26]

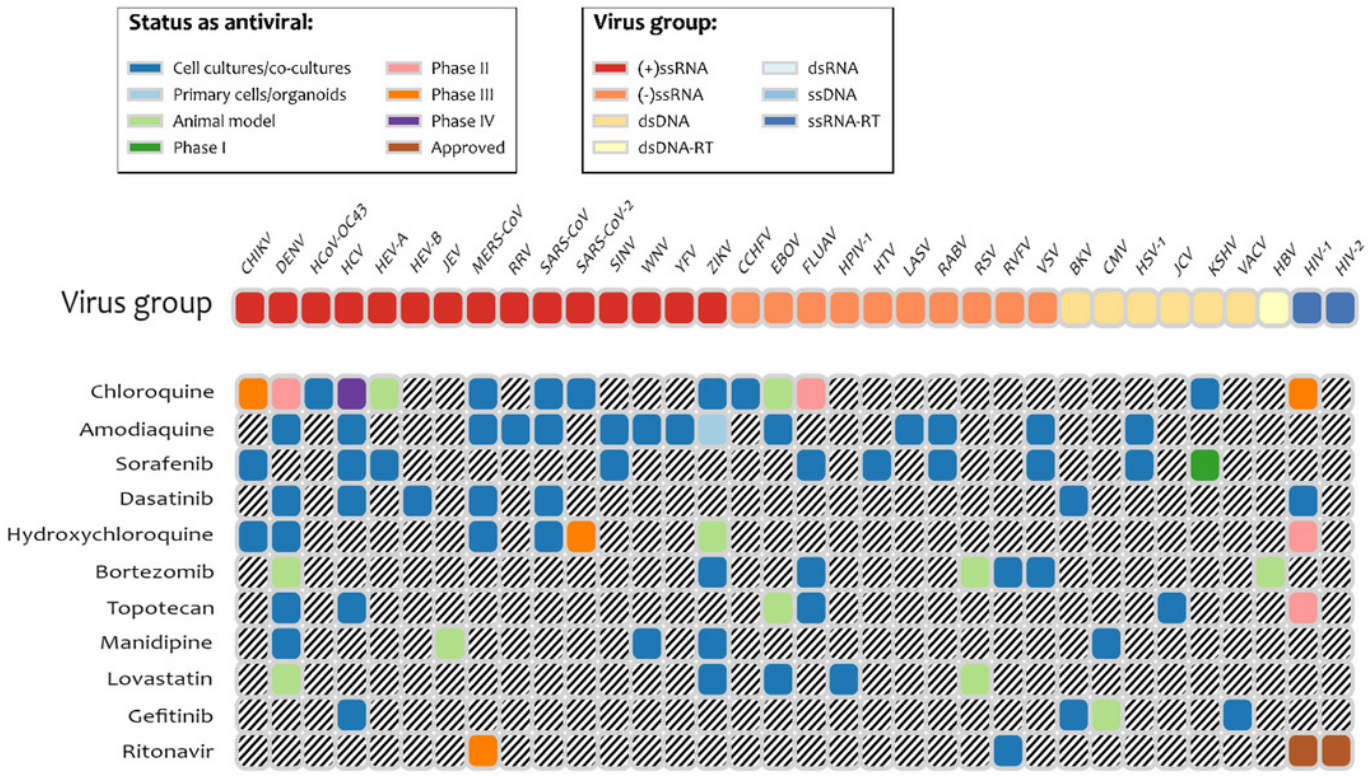

Table 1(on next page)

Drug-candidates clustered by fingerprint similarity–overlap alignment.

Table 1. Drug-candidates clustered by fingerprint similarity–overlap alignment.

Cluster						
A	**B**	**C**	**D**	**E**	**F**	**G**
Alclometasone	Abemaciclib	Bilastine	Dipyridamole	Acebutolol	Isoetharine	Lactulose
alpha-Tocopherol acetate	Bosentan	Darifenacin	Enoxacin	Atenolol	Isoxsuprine	Micronomicin
Bimatoprost	Cefdinir	Droperidol	Gatifloxacin	Betaxolol	Nylidrin	Netilmicin
Boceprevir	Cefmenoxime	Fluspirilene	Gemifloxacin	Bisoprolol	Protokylol	Tobramycin
Buprenorphine	Cefmetazole	Haloperidol	Moxifloxacin	Celiprolol		
Calcitriol	Cefotaxime	Iloperidone		Esmolol		
Diflorasone	Cefotiam	Loperamide		Metipranolol		
Dihydroergocryptine	Cephaloglycin	Ropinirole		Metoprolol		
Flunisolide	Copanlisib	Ziprasidone		Nadolol		
Fluocinolone acetonide	Dasatinib			Propafenone		
Ibutilide	Dicloxacillin					
Iloprost	Doxazosin					
Lapyrium	Enasidenib					
Lovastatin	Flucloxacillin					
Methyl undecenoyl leucinate	Gefitinib					
Retapamulin	Latamoxef					
Ritonavir	Nilotinib					
Travoprost	Prazosin					
Vitamin E Succinate	Riociguat					
Zucapsaicin	Vemurafenib					

Table 2(on next page)

List of docked compounds sorted by their energies of interaction with COVID-19 papain-like protease in the docked positions

Table 2. List of docked compounds sorted by their energies of interaction with COVID-19 papain-like protease in the docked positions

Drug name	DFE* energy	Cluster	Drug name	DFE* energy	Cluster
Nilotinib	-9.3	B	Losartan	-7.3	aa
Irinotecan	-8.5	S	Tolvaptan	-7.3	S
Levomefolic acid	-8.4	S	Darifenacin	-7.3	C
Enasidenib	-8.1	B	Flunisolide	-7.3	A
Siponimod	-8.0	S	Alvimopan	-7.2	hh
Sorafenib	-8.0	S	Iloperidone	-7.2	C
Dihydroergocryptine	-8.0	A	Indacaterol	-7.2	S
Abemaciclib	-7.9	B	Mirabegron	-7.2	S
Ziprasidone	-7.9	C	Ximelagatran	-7.2	S
Pemetrexed	-7.8	hh	Droperidol	-7.2	C
Doxazosin	-7.8	B	Ertapenem	-7.2	jj
Axitinib	-7.7	S	Ivacaftor	-7.1	S
Indinavir	-7.7	S	Loperamide	-7.1	C
Lymecycline	-7.7	S	Flibanserin	-7.1	S
Methysergide	-7.7	I	Brexpiprazole	-7.0	C
Rutin	-7.7	S	Cefmenoxime	-7.0	B
Vemurafenib	-7.7	B	Latamoxef	-7.0	B
Glyburide	-7.7	dd	Olmesartan	-7.0	aa
Trabectedin	-7.6	S	Bilastine	-6.9	C
Dasatinib	-7.6	B	Bosentan	-6.9	C
Methylergonovine	-7.5	I	Cefdinir	-6.9	C
Riociguat	-7.5	B	Cefotaxime	-6.9	B
Fluocinolone	-7.5	A	Prazosin	-6.9	B
Fluspirilene	-7.5	C	Retapamulin	-6.9	A
Isavuconazole	-7.4	S	Ritonavir	-6.9	A
Manidipine	-7.4	ii	Sulfasalazine	-6.9	S
Regadenoson	-7.4	S	Topotecan	-6.9	H
Glimepiride	-7.4	dd	Copanlisib	-6.9	B
Canagliflozin	-7.3	bb	Diflorasone	-6.9	A
			Gemifloxacin	-6.9	H

*Docking free energy; S- single compound cluster